Simplified analytical fracture mechanics model for the evaluation of concrete cone capacity of a single headed stud and experimental validation on anchors with various embedment depths

Miora Nirina Robson, Amine Lahouar, Omar Al-Mansouri, Nicolas Pinoteau, Roberto Piccinin, Marco Abate, Sébastien Rémond, Dashnor Hoxha

Simplified analytical fracture mechanics model for the evaluation of concrete cone capacity of a single headed stud and experimental validation on anchors with various embedment depths

Miora Nirina Robson[1,3 *], Amine Lahouar[1], Omar Al-Mansouri[1], Nicolas Pinoteau[1], Roberto Piccinin[2], Marco Abate[2], Sébastien Remond[3], Dashnor Hoxha[3]

1. Université Paris-Est, Centre Scientifique et Technique du Bâtiment (CSTB), Champs-sur-Marne, France
2. Hilti Corp., Schaan, Principality of Liechtenstein, Liechtenstein
3. Univ Orléans, Univ Tours, INSA CVL, LaMé, EA 7494, France

[*]Corresponding author email: mioranirina.robson@cstb.fr

Abstract

In structural engineering applications, cast-in place steel headed studs are commonly used to transfer external loads to concrete members. When subjected to a tensile load, a single headed stud placed far from concrete edges and adjacent anchors is likely to fail by pulling out a cone-shaped concrete chunk. To determine the concrete cone failure load of a single headed stud, most of the current design-oriented documents adopt the well-known Concrete Capacity Design (CCD) method. This method is user-friendly for engineers, as the only required entry data are the anchor embedment depth and the compressive strength of the concrete. However, as this method was mainly derived from regression analyses of experimental results obtained at room temperature, it might not be suitable for conditions where concrete has been exposed to high temperature. In this paper, a simplified theoretical model using fracture mechanics theory to describe the concrete cone capacity of a single headed stud at room temperature is presented. Then, the accuracy of the model for four different embedment depths is verified. In the model, hypothesis and simplifications are made on the basis of the failure mechanism, and the controlling material parameters are the fracture energy and Young's modulus of concrete. This approach is advantageous for its simplicity without, however, losing the description of the failure mechanism. Confrontation of the predictions of the model to experimental results yielded good agreement for all embedment depths. This analytical model could be used for future development of prediction methods in special contexts, such as the presence of thermal loading.

Keywords: *concrete cone, headed stud, fracture mechanics, energy balance, analytical model*

1. Introduction

Anchoring systems are an engineering solution allowing to transfer load from external elements to concrete. In general, they can be classified as either cast-in-place anchors or post-installed anchors. The first category corresponds to anchors that are secured in the formwork prior to casting the concrete, whereas the second category consists of anchors installed in hardened concrete after casting (Eligehausen et al. 2006). Among cast-in-place anchors, headed studs are commonly used. When loaded in tension, a headed stud experiences one of the following failure modes: steel failure, concrete cone failure, concrete splitting, pull out failure and lateral blow out failure (EN 1992-4 2018) (Eligehausen et al. 2006). The concrete cone failure is characterized by the formation of a cone-shaped fracture surface in concrete.

Several investigations have been performed over the past few decades to explain and characterize the mechanism of a concrete cone failure and to determine the failure load (Ottosen 1981) (Elfgren et al. 1982) (Krenchel and Shah 1985) (Eligehausen and Sawade 1989) (Elfgren et al. 2001). It can be deduced from these studies that when a headed stud is loaded in tension, high circumferential tensile stresses develop around the point where load is introduced in the concrete. Subsequently, microcracks and circumferential tensile cracks are initiating at the head of the anchor. As the load increases, these cracks

propagate towards the concrete surface. This propagation is stable during a first step but becomes unstable when the ultimate load is reached. At the ultimate load, the circumferential cracks reach only 40% to 50% of the full apothem of the final cone (Eligehausen and Sawade 1989). Moreover, the slope of the cone envelope varies between 30° to 40° with respect to the surface of the concrete component. On average it is about 35°, however, it has the tendency to increase with embedment depth (Zhao 1993). In addition, recent investigations showed that the failure angle also increases with anchor head size (Nilforoush et al. 2017) (Nilforoush et al. 2018).

At the present, most of the design-oriented documents at international level (EN 1992-4-2018) (fib Model Code for Concrete Structures 2010) (ACI-318-19) are derived from the well known CCD method (Fuchs et al. 1995) for the evaluation of the concrete cone capacity of anchors. According to this method, the mean concrete cone capacity of a headed stud unaffected by neighboring anchors or nearby concrete edges is given by (1):

$$F_{CCD} = 15.5 \sqrt{f_{cc}}\, h_{ef}^{1.5} \tag{1}$$

In (1), f_{cc} [MPa] is the compressive strength of concrete based on 150 mm cubes and h_{ef} [mm] is the effective embedment depth measured between concrete surface and top corner of the anchor head. Therefore, the 15.5 factor takes dimensional units of [$N^{0.5}/mm^{0.5}$]. According to (Fuchs et al. 1995), the term $\sqrt{f_{cc}}$ indicates that the concrete tensile strength is proportional to the square root of the concrete compressive strength. Besides, the term $h_{ef}^{1.5}$ signifies that the ultimate load is proportional to the total failure area and affected by a size effect. Indeed, at ultimate load, if the embedment is increased, the stress obtained by dividing the ultimate load to the idealized concrete cone surface is decreasing. As for the coefficient 15.5 in (1), it was derived empirically from regression analyses of 318 individual tests carried on headed studs of different embedment depths cast in specimens of varying strength (Rehm et al. 1988)(Fuchs et al. 1995). However, no clear relationship can be established between compressive strength and fracture energy of concrete (Kozul and Darwin 1997). Therefore, it may be said that despite its user-friendly aspect, (1) does not indicate explicitly the dependence of the concrete cone capacity on the failure mechanism.

To study the effect of fracture properties on the concrete cone ultimate load-bearing capacity, a numerical study on the influence of the concrete tensile strength f_t and the concrete fracture energy G_F was performed (Eligehausen 1991). The results indicated that for a given fracture energy, the ultimate load increases slightly with the concrete tensile strength. However, for a given concrete tensile strength, the concrete cone failure load increases considerably with the fracture energy. Moreover, this increase is roughly proportional to $G_F^{0.5}$. This is coherent with Sawade's energy-based equation (2), which suggest the dependence of the failure load on the fracture energy G_F and Young's modulus E of concrete. This energy model was based on Linear Elastic Fracture Mechanics and used numerical simulations to identify the dimensionless coefficient 2.1 (Sawade 1994).

$$F_{Sawade} = 2.1 \sqrt{E G_F}\, h_{ef}^{1.5} \tag{2}$$

The present investigation consists in evaluating analytically the concrete cone capacity of a single headed stud using a simple representation of the failure mechanism. An experimental investigation to assess the validity of this simplified model is presented. The test results are also compared to the predictions of CCD method and Sawade's model to assess their practical validity.

2. Description of the analytical model

Fracture mechanics theory studies the mechanical behaviour of cracked bodies subjected to an applied load, and allows to determine the maximum admissible stress for a given crack size, or to determine the maximum admissible crack size given an applied load. For the application to the concrete cone capacity, the goal is to predict the failure load. For a concrete-like loaded cracked body, the sum of the potential

energy, W_{pot} , and the surface energy from macro crack growth, W_{crack} , could be written as a difference between the work of internal forces, W_{int} , and external forces, W_{ext} , (3)(4):

$$W_{pot} + W_{crack} = W_{int} - W_{ext} = W_{el} + W_{FPZ} - W_{ext} \quad (3)$$

$$W_{pot} = W_{el} - W_{crack} + W_{FPZ} - W_{ext} \quad (4)$$

where, W_{el} is the elastic strain energy, W_{FPZ} is the fracture process zone (FPZ) energy where any other dissipative phenomena such as matrix microcracking, debonding of matrix-aggregate interface and eventual plastic yielding can be observed. Therefore, the minimum of potential energy principle in cracking process reads (5):

$$\frac{\partial W_{pot}}{\partial A} = -\frac{\partial \mathrm{W_{ext}}}{\partial A} + \frac{\partial W_{el}}{\partial A} - \frac{\partial W_{crack}}{\partial A} + \frac{\partial W_{FPZ}}{\partial A} = 0 \quad (5)$$

To obtain a simple expression for the strength, without a description of the stable crack propagation nor of the FPZ developing, the analysis can be focused on a hypothetical situation when the pull-out test is conducted up to the critical crack length and is immediately unloaded to avoid the failure. If the pre-cracked sample is reloaded, the full reloading process up to critical crack length becomes elastic. Therefore, for the reloading elastic process, the area under load-displacement curve is exactly the half of the work of external load i.e. the work of external load is the double of the elastic energy. In addition, after stable crack propagation in concrete, the FPZ energy becomes negligible compared to crack energy due to a drop of FPZ size (Kim et al. 2020). Finally, the classical energy release rate equation is obtained (6):

$$\frac{\partial W_{el}}{\partial A} = -\frac{\partial W_{crack}}{\partial A} \quad (6)$$

To evaluate W_{el} and W_{crack} at this stage, the fundamental idea consists in applying brittle materials theory, as the concrete shows a pure brittle material behaviour from the instability point. In one hand, W_{crack} is evaluated with considering an invariant surface energy equal to the so-called fracture energy G_F of concrete, giving $W_{crack} = G_F(\pi a^2 \cos\beta)$. In the other hand, W_{el} is evaluated using a simplification for brittle materials. For a crack of length 2a in an infinite plate remotely loaded by stress σ, Perez (2017), showed that energy released is equal to that of a uniform density energy stored in two cylinders of radii equal to half of the crack length. Similar results, implying however a corrective factor close to $4/\pi^2$ could be obtained for a penny-shaped crack with cylinders replaced by a torus of section radius equal to that of the penny shaped crack and enveloping the crack edge. Therefore, transposition to the case of a cone-shaped crack suggests that the energy release zone would have the equivalent size of a torus shaped volume element surrounding the crack tip (Fig. 1). Therefore, the released energy reads $W_{el} = (\int \sigma d\varepsilon)(4\pi^2 a^3 \cos\beta)$.

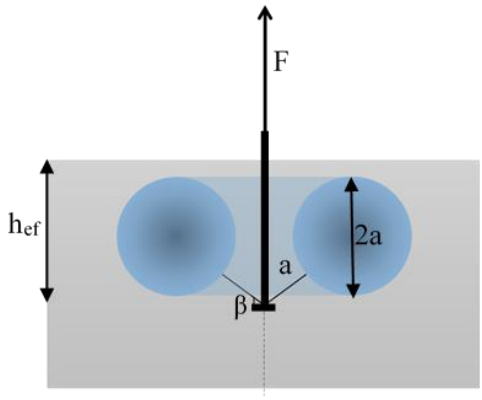

Figure 1: Equivalent torus-shaped energy release zone

Hence, with a cone shaped crack surface proportional to the crack length a, the conservation of energy variation due to the displacements arising from the crack length change ∂a can be defined as (7):

$$\frac{\partial(\sigma d\varepsilon)\,(4\pi^2 a^3 cos\beta)}{\partial a} = -\frac{\partial G_F(\pi a^2 cos\beta)}{\partial a} \tag{7}$$

Moreover, the strain energy density can be expressed using Hook's law, with a normal stress σ assumed to act over the crack region as $\sigma = F\cos\beta/\pi a^2\cos\beta$. Therefore, the expression of the load is obtained after derivations as (8):

$$F = \sqrt{\pi a^3 E G_F} \tag{8}$$

At failure, the crack length has its critical value a_{cr} which is presumed to be approximately 45% of the slant height of the final cone (Eligehausen and Sawade 1989), hence $a_{cr} \approx 0.45l \approx 0.45h_{ef}/\sin\beta$. Therefore, the ultimate load can be expressed as a function of the embedment depth and the failure angle as (9):

$$F = \sqrt{\frac{0.45^3\pi}{(sin\beta)^3}}\sqrt{E G_F}\, h_{ef}^{1.5} \tag{9}$$

If the failure angle is assumed to have an average value β=35° as suggested in past investigations (Zhao 1993) (Fuchs et al. 1995), the ultimate load F_{max} at failure would finally read (10):

$$F_{max} \approx 1.23\sqrt{E G_F}\, h_{ef}^{1.5} \tag{10}$$

3. Description of the tests

3.1. Test specimens

The type of headed stud considered in this experimental campaign consisted of M16 threaded rods with 2 mm threads, welded to a nut and a washer whose characteristics are shown in Figure 2. For each component, carbon steel of grade 10.9 has been used (ISO 898-1-2009) and the mean ultimate tensile strength of the threaded rod was f_u = 1280 MPa.

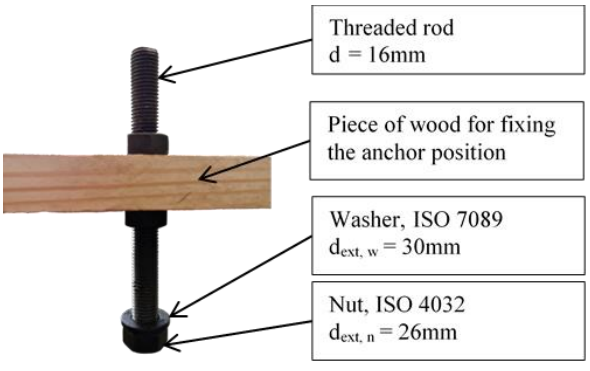

Figure 2: Characteristics of the headed stud

Four values of the embedment depth h_{ef} have been considered (Tab. 1). For each embedment depth, three tests have been carried out to ensure a good reproducibility. The total of 12 headed studs were cast in a common large reinforced concrete slab 2.5 m long, 1.4 m wide and 0.4 m thick. Their positions have been chosen to avoid overlap of each individual concrete cone, based on the design method in (EN 1992-4).

Table 1. Embedment depths and number of tested headed studs

h_{ef}	Number
57 mm ±5.3%	3
81 mm ±1.6%	3
108 mm ±2.2%	3
136 mm ±1%	3

The concrete material used to construct the slab was a ready-mix concrete of class C25/30 with a maximum aggregate size of 13.5 mm. Table 2 presents the composition of the concrete and the average values of its mechanical properties. The pull-out tests and the characterization of concrete mechanical properties were performed after a minimum of 35 days from casting. The compressive strength of concrete was measured on additional concrete cubes (side: 150 mm) in accordance with EN 12390-3. Likewise, the tensile strength was measured on cylinders (diameter: 160 mm; height: 320 mm) in accordance with EN 12390-6. In addition, Young's modulus of concrete was characterized following EN 12390-13 and the concrete fracture energy was measured by means of a three-point bending test on standard concrete notched prisms (length: 600 mm, width: 150 mm, height: 150 mm), in accordance with RILEM TC 162-TDF 2002 (RILEM 2002).

Table 2: Properties of concrete

Cement proportion	286 kg/m^3
Water/Cement ratio	0.54
Aggregate/Sand ratio	1.06
Compressive strength f_{cc}	33.1 MPa
Tensile strength f_t	3.2 MPa
Young's modulus E	27.6 GPa
Fracture energy G_F	96.5 J/m²

3.2. Test setup and test process at room temperature

Figure 3 shows the test setup adopted for the pull-out tests following the recommendations of corresponding assessment document (EAD 330232-01-0601).

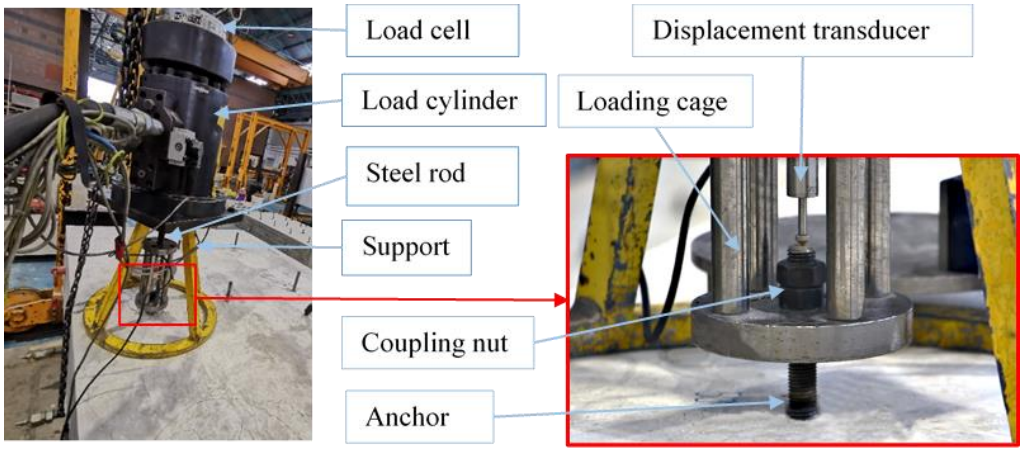

Figure 3: Concrete breakout test setup/unconfined tension test acc. EAD 330232, 2016

A displacement-controlled system was chosen to capture the post-peak behaviour of the anchor. The loading was applied to the anchor using a hydraulic jack with a maximum capacity of 200 kN. The jack transferred the load through a high-strength steel rod, which was connected to a hollow cylinder cage, connected to the free end of the anchor by two coupling nuts. To prevent the vertical movement of the slab, the jack was supported by a steel support which rested directly on the slab. The dimension of the

support was chosen sufficiently large, i.e. a diameter larger than $4h_{ef}$ to allow the formation of an unrestricted cone. The applied load was measured by a load cell placed on the top of the load cylinder. For measuring the anchor displacement, a linear variable differential transformer (LVDT) was installed on the top of the anchor, in such a way that its axis and that of the anchor coincide.

4. Test results and discussions

4.1. Load displacement curves

For all performed tests, the evolutions of the measured tensile load F with the measured displacement of the anchor are summarized in Figure 4. It may be observed from the load-displacement curves that before the ultimate load, each curve consists on a short first part slightly linear and then a second part non-linear until the ultimate load. The first part corresponds to low loads not sufficient to create a crack. The passage to the non-linear phase may suggest the beginning of a stable crack growth and the development of the Fracture Process Zone. It can also be seen on the curves that the stiffness is decreasing during the non-linear phase, which may indicate an additional displacement resulting from microcracking. Moreover, the load decreases suddenly after ultimate load, which is coherent with the consideration of a post-peak quasi-brittle failure.

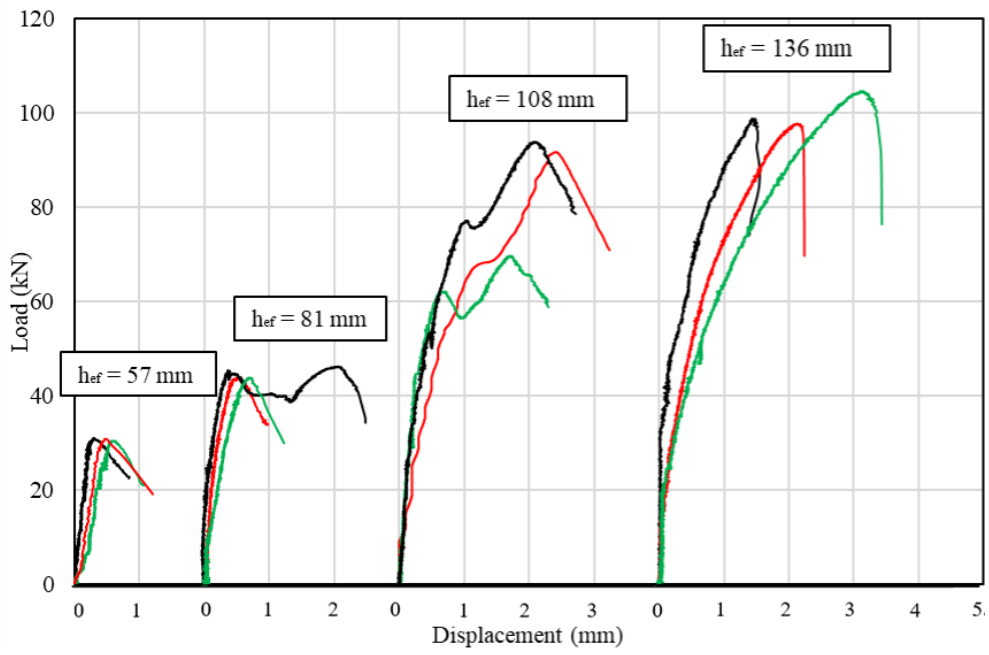

Figure 4: Load-displacement curves

Besides, the displacement at ultimate load seems to be greater for the two deepest embedment depths, suggesting a higher degradation of the stiffness at failure, i.e. a greater damage linked to a larger crack surface and/or a larger Fracture Process Zone. This seems to confirm that the critical crack length is proportional to the embedment depth of the anchor.

4.2. Failure mechanism and crack patterns

During the loading and until the ultimate load was reached, no crack was observed on the surface of the slab. As expected, all anchors underwent concrete cone failure. However, the extracted cones were sometimes split into separated pieces, which may indicate the formation of radial cracks. The failure angle of the extracted cones varied between 25° and 40°. In addition to a variation from one test to another, the variation of the failure angle was also observed within the same failure cone whether it was

along the failure crack or depending on the viewing angle. Photos of a failure cone taken from two different sides of the same failure cone with one of the shallowest anchors h_{ef} = 57 mm are shown on Figure 5. Moreover, measurements seemed to show that the failure angle slightly increase with embedment depth.

Figure 5: Typical failure cone

4.3. Ultimate loads and comparison with prediction models

Table 3 gives the summary of ultimate load $F_{u,i}$ obtained with each individual test as well as the mean ultimate load $F_{u,m}$ per embedment depth. The coefficient of variations (COV) associated to the mean ultimate loads $F_{u,m}$ are also given to have indication on the scatter of the tests results.

Table 3. Ultimate loads

h_{ef} (mm)	Number of tests	$F_{u,i}$ (kN)	$F_{u,m}$ (kN) (COV)
57	3	30.85	30.77 (1.00 %)
		31.03	
		30.43	
81	3	43.81	44.62 (2.04 %)
		46.2	
		43.84	
108	3	91.68	85.07 (15.72%)
		69.68	
		93.84	
136	3	98.79	100.38 (3.68%)
		97.75	
		104.61	

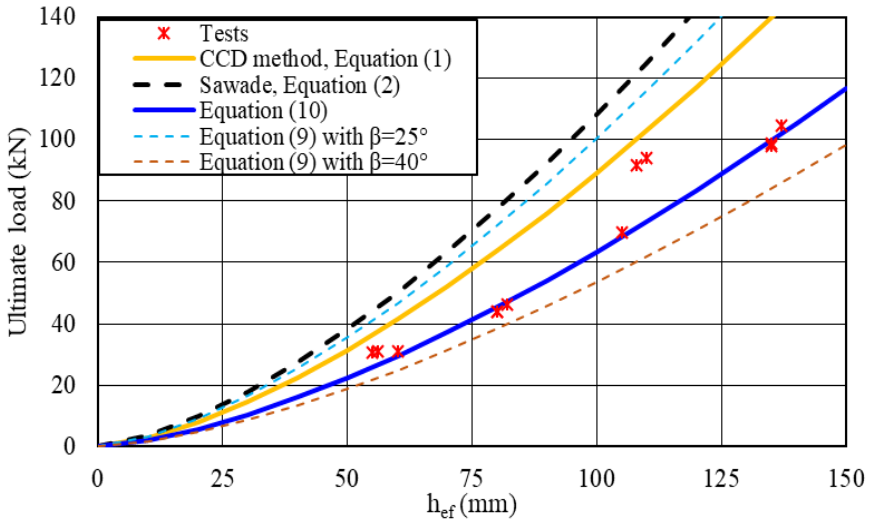

Figure 6: Comparison between experimental ultimate loads and models predictions

Figure 6 shows the comparison of the ultimate loads $F_{u,m}$ with the existing equations (1) and (2) as well as the proposed analytical equation (10). In addition, the predictions of the analytical equation (9) using the minimum measured failure angle of 25° and the maximum measured angle of 40° are presented.
It may be observed in Figure 6 that the CCD method and Sawade's equations give predictions close to the experimental results, despite a slight overestimation as could be observed in past studies (Eligehausen et al. 2006) (Eligehausen and Sawade 1989). It can also be seen that the prediction of the analytical equation (10) provides a good agreement with the data, except for h_{ef} = 108 mm, for which the larger scatter shown in Table 3 does not allow a conclusive statement. Moreover, the test results as well as the prediction of CCD method lie between the boundary values predicted by the analytical equation (9) using the minimum and the maximum measured failure angles. The upper limit obtained with the minimum failure angle $\beta = 25°$ is close to the prediction of the existing equations (1) and (2). These results seem to suggest that the use of the concrete fracture parameters is suitable for the evaluation of the concrete cone capacity. In this study, a failure angle $\beta = 35°$ seems to give a good fit of the test data. However, the cracking of concrete may depend on the arrangement and the characteristics of aggregates and the cement matrix. Therefore, further investigation would be necessary to assess if the analytical equation is still appropriate with other concrete formulations.

4. Concluding remarks

This paper presents an investigation of the concrete cone capacity of a single headed stud at room temperature with consideration of the failure mechanism. A simplified theoretical development using energy-based Linear Elastic Fracture Mechanics was established to evaluate the concrete cone ultimate capacity. The analysis was done considering a hypothetical moment at the end of the stable crack growth, and relies on the following main assumptions:

- At the onset of unstable crack growth, concrete behaves similarly to an elastic pure brittle material with an invariant fracture energy $G_{F.}$
- As a generalisation of Perez's suggestions, the energy release is represented by the uniform strain energy stored into a torus of radius equal to the crack length.
- The failure angle is around 35° and the stable crack growth ends when the crack length is approximately 45% of the total failure cone apothem.

An experimental program to assess the validity of the prediction of the proposed model with regard to four values of embedment depths was then presented. Moreover, test results were confronted to the main existing models in literature. The results may call for the following observations:

- The load-displacement curves transcribe the failure mechanism by showing the three main steps of a concrete cone failure: a first elastic short part, a second nonlinear part corresponding to stable crack growth with FPZ development and a progressive decrease of stiffness, and an unstable crack propagation phase with rapid decrease of the capacity after the ultimate load.
- The failure angle varies from 25° to 40° depending on the test, on the angle of view around a failure cone, and on the measurement point along the crack path. Moreover, the angle seemed to increase with embedment depth.
- The proposed model seems to be in good agreement with the tests results in almost all cases compared to existing equations. This may highlight that the concrete cone capacity is better represented with the fracture parameters of concrete. However, as the experimental program investigated only one type of concrete formulation, further investigation will follow to assess the accuracy of the model with different concrete formulations.

Acknowledgements

The authors want to thank the technical team of the CSTB: Etienne Bruchet, Killian Regnier, Julie Skorupka, Jean Christophe Caillot and Hubert Auster for their contribution to the preparation of the specimens and the execution of the tests.

Copyright

References

ACI CODE-318-19: Building Code Requirements for Structural Concrete and Commentary.

AFNOR. *Norme NF EN 12390-3 Essai pour béton durci. Partie 3 : résistance à la compression des éprouvettes - AFNOR*.

Elfgren, Lennart, Krister Cederwall, Kent Gylltoft, et Carl Erik Broms. 1982. Fatigue of Anchor Bolts in Reinforced Concrete Foundations. In International Association for Bridge and Structural Engineering, 463-70.

Elfgren, Lennart, Rolf Eligehausen, et J. Rots. 2001. Anchor bolts in concrete structures: Summary of round robin tests and analysis arranged by RILEM TC 90-FMA “Fracture Mechanics of Concrete - Applications”. *Materials and Structures* 34: 451-57.

Eligehausen, Rolf. 1991. Use of the Tensile Strength in Anchorage to Concrete. https://www.academia.edu/30637930/Use_of_the_tensile_strength_in_anchorage_to_concrete (7 avril 2020).

Eligehausen, Rolf, Rainer Mallée, et John F. Silva. 2006. *Anchorage in Concrete Construction*. John Wiley & Sons.

Eligehausen, Rolf, et Gottfried Sawade. 1989. A Fracture Mechanics Based Description of the Pull-out Behavior of Headed Studs Embedded in Concrete. http://elib.uni-stuttgart.de/handle/11682/7947

EOTA. 2016. EAD 330232-01-0601. Mechanical fasteners for use in concrete.

fib Model Code for Concrete Structures 2010 - Ernst-und-Sohn.de. https://www.ernst-und-sohn.de/index.php?q=en/fib-model-code-for-concrete-structures-2010 (21 janvier 2021).

Fuchs, Werner, Rolf Eligehausen, et John E. Breen. 1995. Concrete capacity design (CCD) approach for fastening to concrete. *ACI Structural Journal* 92(1): 73-94.

ISO 898-1. 2009. https://norminfo.afnor.org/norme/NF%20EN%20ISO%20898-1/caracteristiques-mecaniques-des-elements-de-fixation-en-acier-au-carbone-et-en-acier-allie-partie-1-vis-goujons-et-tiges/103590

Kim, Seong-Kyum, Ho Geun Shin, Suman Timilsina, et Ji Sik Kim. 2020. Determining the Fracture Process Zone Length and Mode I Stress Intensity Factor in Concrete Structures via Mechanoluminescent Technology. *Sensors (Basel, Switzerland)* 20(5). https://www.ncbi.nlm.nih.gov/pmc/articles/PMC7085635/ (19 octobre 2020).

Kozul, Rozalija, et D. Darwin. 1997. Effects of Aggregate Type, Size, and Content on Concrete Strength and Fracture Energy.

Krenchel, H., et S. P. Shah. 1985. Fracture Analysis of the Pullout Test. *Materials and Structures* 18(6): 439-46.

EN 1992-4 - Septembre 2018. https://www.boutique.afnor.org/norme/nf-en-1992-4/eurocode-2-calcul-des-structures-en-beton-partie-4-conception-et-calcul-des-elements-de-fixation-pour-beton/article/818166/fa183514 (21 août 2020).

EN 12390-13, P18-430-13 (02/2014). *Normadoc*. https://www.normadoc.com/french/nf-p18-430-13-nf-en-12390-13-02-2014.html.

Nilforoush, Rasoul, Martin Nilsson, et Lennart Elfgren. 2017. Experimental Evaluation of Tensile Behaviour of Single Cast-in-Place Anchor Bolts in Plain and Steel Fibre-Reinforced Normal- and High-Strength Concrete. *Engineering Structures* 147: 195-206.

———. 2018. Experimental Evaluation of Influence of Member Thickness, Anchor-Head Size, and Orthogonal Surface Reinforcement on the Tensile Capacity of Headed Anchors in Uncracked Concrete. *Journal of Structural Engineering* 144(4): 04018012.

EN 12390-6 Essai pour béton durci. Partie 6 : résistance en traction par fendage d’éprouvettes - AFNOR. https://www.decitre.fr/livres/norme-nf-en-12390-6-essai-pour-beton-durci-5552120003652.html

Ottosen, Niels Saabye. 1981. Nonlinear Finite Element Analysis of Pull-Out Test. *Journal of the Structural Division* 107(4): 591-603.

Rehm, Gallus, Rolf Eligehausen, et Rainer Mallée. 1988. Befestigungstechnik

RILEM. 2002. RILEM TC 162-TDF: TEST AND DESIGN METHODS FOR STEEL FIBRE REINFORCED CONCRETE. https://www.rilem.net/images/publis/1384.pdf

Sawade, Gottfried. 1994. Ein energetisches Materialmodell zur Berechnung des Tragverhaltens von zugbeanspruchtem Beton .

Zhao, Guochen. 1993. Tragverhalten von randfernen Kopfbolzen-verankerungen bei Betonbruch.